J Mater Sci (2015) 50:6526–6530
DOI 10.1007/s10853-015-9215-6

Magnetic characteristics of $Tb_x(FeCoV)_{100-x}$ films

Tangfu Feng[1] · S. Yu[1] · R. B. Sun[1] · F. Y. Kong[1] · F. Wang[1] · J. Z. Wang[1]

Received: 6 May 2015 / Accepted: 26 June 2015 / Published online: 3 July 2015

Abstract The magnetic characteristics of TbFeCoV films deposited at different sputtering conditions were investigated using magnetic force microscope, vibrating sample magnetometer and other testing equipments. A minimum out-of-plane saturation magnetization and a maximum out-of-plane coercivity were obtained for the $Tb_x(FeCoV)_{100-x}$ films near the point of compensation $x = 23$. As $x = 23$–45, perpendicular magnetization component could be observed, while the second largest saturation magnetization and a relatively low coercivity were obtained in the $x = 40$ sample. For the amorphous $Tb_{40}(FeCoV)_{60}$ films, with the increase of sputtering pressure or power, the out-of-plane saturation magnetization increases to a maximum and then decreases while the out-of-plane coercivity shows a monotonously decreasing trend as sputtering power is increased from 43 to 64 W. The change of perpendicular magnetic anisotropy can be confirmed by the difference of magnetic domain for the samples deposited at different sputtering pressures or powers.

Introduction

Rare-earth–transition metal (RE–TM) TbFe alloy films are considered to be promising materials used in electromechanical transducer devices [1, 2]. A large effort has been made to fabricate TbFe(Co) films with reduced coercivity and controlled the easy direction of magnetization by magnetron sputtering [3, 4]. For Tb_xFe_{100-x} films, as $x = 25$–45, it produces perpendicular magnetic anisotropy (PMA), a large coercive field and a high saturation magnetization [5]. These properties can be controlled by adjusting the process parameters during sputtering such as working pressure and substrate temperature [6, 7]. Yet, few attempts have been made to conduct a systematic research on TbFeCoV films, especially regarding magnetic domain variation with sputtering pressure and power.

In this work, we studied systematically the dependence of magnetic characteristics on sputtering pressure and power for the $Tb_x(Fe_{49}Co_{49}V_2)_{100-x}$ films. It was found that a strong PMA was obtained at an optimum deposition condition and underlying mechanism is discussed.

Experimental details

The $Tb_x(FeCoV)_{100-x}$ films were dc magnetron co-sputtered from a multiple target arrangement with a pure Tb target and a composite $Fe_{49}Co_{49}V_2$ target (America: Hiperco50, Russia: 50 KΦ, China: 1J22) onto Si (100) substrates. The crystallographic properties and the composition were characterized by X-ray diffraction (XRD) and field-emission scanning electron microscope (FE-SEM), respectively. The magnetic domain structure was explored by magnetic force microscope in tapping/lift modes (MFM). The magnetic measurement was carried out on a vibrating sample magnetometer (VSM).

✉ Tangfu Feng
ftf1028@126.com

[1] School of Materials Science and Engineering, Ningbo University of Technology, Ningbo 315016, China

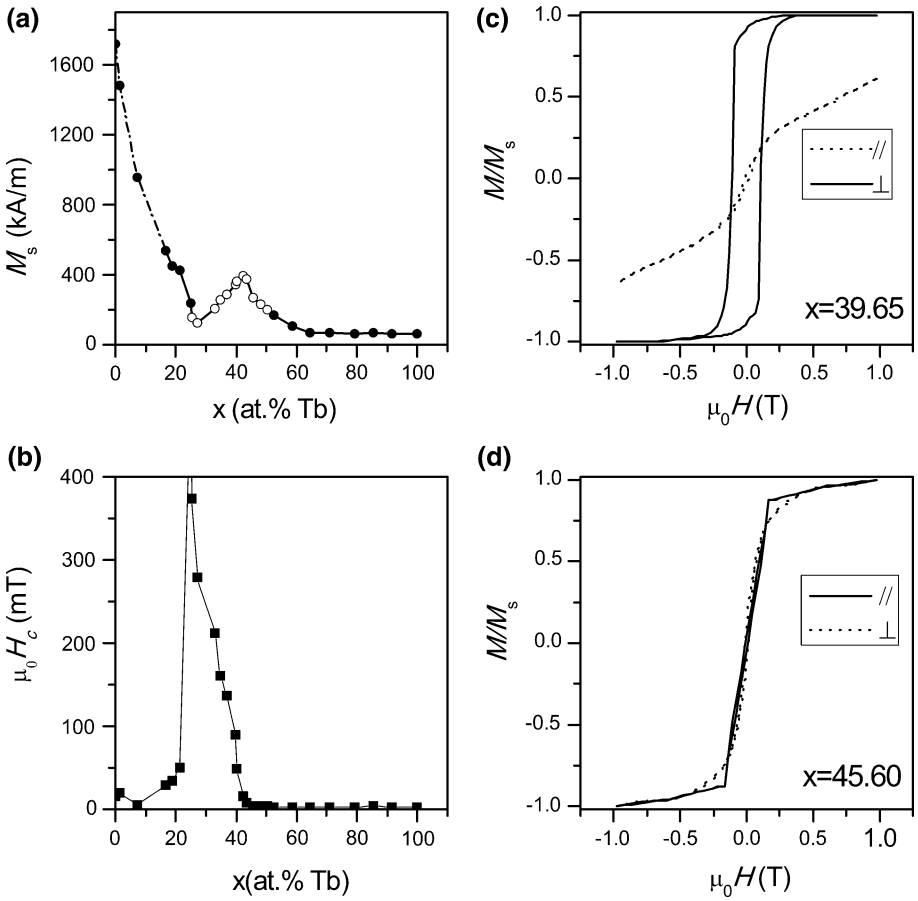

Fig. 1 **a** Saturation magnetization (M_s) and **b** coercivity ($\mu_0 H_c$). **c** Magnetic hysteresis loops at $x = 39.65$ and **d** $x = 45.6$. **a** The *dashed* and *solid curves* denote, respectively, crystallized and amorphous states, while the *open* and *closed circles* denote easy directions of magnetization in the film plane and perpendicular to it

Results and discussion

Magnetic properties of $Tb_x(FeCoV)_{100-x}$ films with different x values

Out-of-plane saturation magnetization (M_s) and coercivity ($\mu_0 H_c$) of as-deposited $Tb_x(FeCoV)_{100-x}$ samples measured at room temperature are shown in Fig. 1.

As can be seen in Fig. 1a, when the value of x increases, the saturation magnetization drops rapidly and becomes almost zero near the point of compensation $x = 23$, and then reaches the second maximum at about $x = 40$. The compensation is a simply cancellation of the two subnetwork moments derived from antiferromagnetic exchange coupling between Tb and Fe(Co) structure [8]. The coercive field first increases and then decreases obviously, which reaches the maximum value of 500 mT at the compensation point, as shown in Fig. 2b. In addition, through comparing hysteresis loops such as Fig. 2a, b, the perpendicular orientation and the hysteresis are weakened with increasing Tb content which is more than composition point ($x > 22$), resulting in a low coercivity of 5.3 mT for $x = 45.6$.

As shown in Fig. 2a–d, with the increase of sputtering Ar pressure, the ratio of Tb in $Tb_x(FeCoV)_{100-x}$ increases because of different sputtering rates in Tb and Fe(Co) atoms; however, the perpendicular orientation and the hysteresis decrease with the increase of it. The increase in Tb content increases the cone angle of sperimagnetism and weakens the coupling between Tb and Fe(Co), which cause perpendicular magnetization anisotropy and coercivity to decrease. Meanwhile, as $x < 40$, the increase of saturation magnetization results from the increase of net moment dominated Tb moment, while the decrease in that results from the weak coupling of Tb and Fe(Co) in $x > 40$ films. At high P_{Ar}, the energy of combining between Tb and Fe(Co) adatoms is weak for the frequent collision of Ar ions/Ar atom and sputtering atoms, which lead to a decline in magnetic coupling between Tb and Fe(Co) atoms. The spherical 4*f* orbital (Tb) could not remained orientation for the weaker coupling between Tb and Fe(Co) moments and then decreases M_s and $\mu_0 H_c$, as shown in Fig. 2e, f. In addition, at high Tb content, the decrease of coercivity results from the superparamagnetism which exhibits the coercivity value of zero both in the in-plane and perpendicular directions [9].

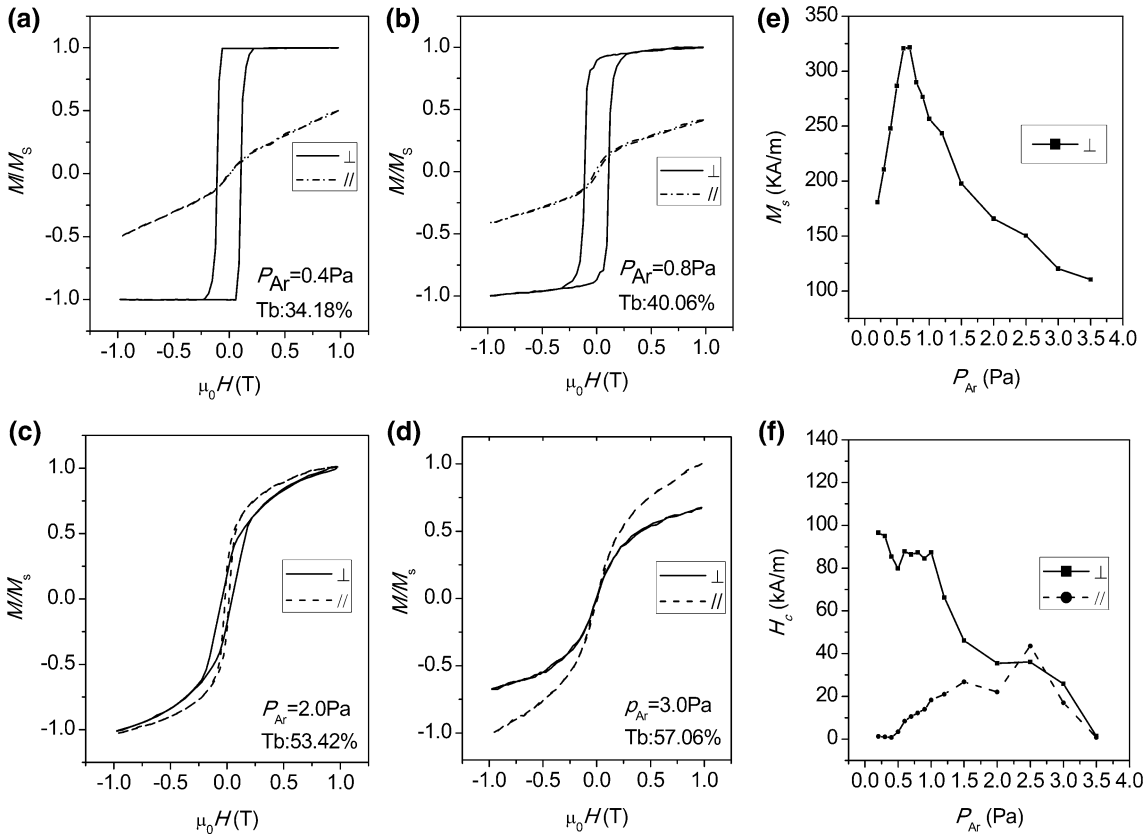

Fig. 2 **a–d** Magnetic hysteresis loops, **e** M_s and **f** $\mu_0 H_c$ for the samples with different components caused by various sputtering pressures

Influence of different sputtering conditions for the $Tb_{40}(FeCoV)_{60}$ films

For the $Tb_x(FeCoV)_{100-x}$ films, as $x \approx 40$, high saturation magnetization and perpendicular magnetization component were obtained, which is shown in Figs. 1 and 2. As shown in Fig. 3, the variation of out-of-plane M_s and $\mu_0 H_c$ with P_{Ar} and P was obtained in the amorphous $Tb_{40}(FeCoV)_{60}$ films. When P_{Ar} increases (Fig. 3a), both the saturation magnetization and coercivity first increase and then decrease, and the maximum of $M_s = 272.5$ kA/m and $\mu_0 H_c = 160.3$ mT are obtained at $P_{Ar} = 0.9$ Pa and $P_{Ar} = 0.8$ Pa, respectively. As can be seen in Fig. 3b, M_s rapidly increases first and then slightly decreases with the increase of P, while $\mu_0 H_c$ shows a monotonous decreasing trend when P is increased from 43 to 64 W.

The variation of magnetic characteristics with the sputtering conditions is more likely to do with pair-order anisotropy (POA) induced by the selective resputtering of surface adatoms during film growth. For the amorphous alloys consisting of rare-earth and transition metals (a-RE–TM) [10], the POA, described as a characteristic for like-atom pairs parallel to the film plane and unlike-atom pairs perpendicular to it, was shown to increase exponentially with PMA. During sputtering at appropriate P_{Ar} and P, the ion/neutral energy within the range of threshold energy is expected to produce the most selective resputtering events and lead to the largest POA, which is denoted by the shaded bar in Fig. 3c [10]. As $P_{Ar} < 0.5$ Pa or $P > 64$ W, one argon ion/neutral incident at the film surface would sputter a surface adatom without a selective character because its energy exceeds threshold energies, while the argon ion/neutral energy is insufficient to overcome the surface work function and no resputtering takes place as $P_{Ar} > 1.5$ Pa or $P < 43$ W. Therefore, when P_{Ar} and P are closed to optimum value, adatoms induced by maximum selective resputtering from the surface of growing film increase the amount of anisotropic atom pairs in film normal direction and thus increase saturation magnetization.

This is also confirmed by domain structures explored using MFM, as shown in Fig. 4. A distinct black–bright contrast strip domain structure is observed for the sample prepared at $P_{Ar} = 0.9$ Pa (Fig. 4b) or $P = 52$ W (Fig. 4f), indicating a strong PMA. For other conditions, the black–bright contrast is gradually degraded, especially, at the high

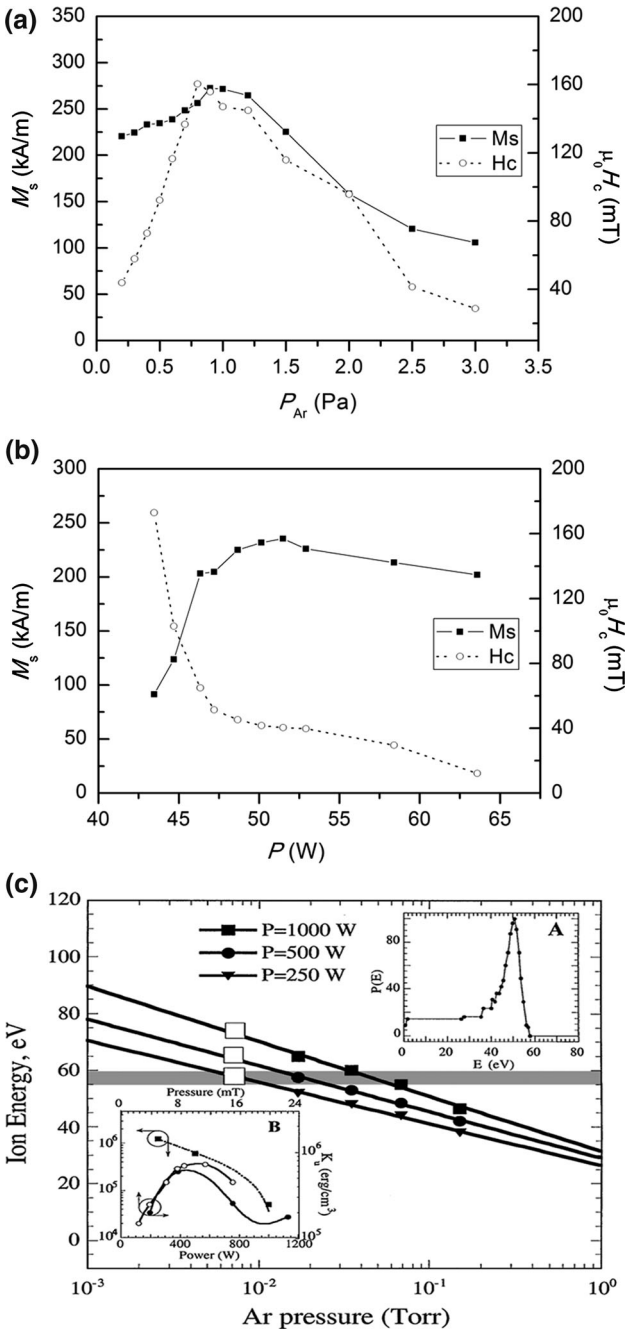

Fig. 3 Variations of out-of-plane $\mu_0 H_c$ and M_s with **a** sputtering pressure P_{Ar}, **b** power P; **c** ion energies versus working gas pressure as a function of rf power [10]

P_{Ar} and low P. This result indicates that the PMA can be dominated by ion/neutral energy-induced sputtering pressure and power. Besides, as shown in Fig. 4f–h, it is observed the magnetic domain shape changes from strip to a combination by strip and small islands and then transformed to maze. These changes may be related to the magnitude and direction of induced stress under different sputtering processes [11, 12], which is still open.

Generally, the coercivity may be connected to the homogeneity and compactness of the metal amorphous films with the same composition [13]. As argon pressure increases from 0.1 to 0.9 Pa, the decrease of binding energy between adatoms decreases compactness and simultaneously increases inhomogeneous regions, which results in increase of defects. These defects would hinder magnetization switching by pinning the domain wall, resulting in a large $\mu_0 H_c$ at a high P_{Ar}. Moreover, with increasing of P_{Ar}, the enhancing PMA causes $\mu_0 H_c$ to increase, as shown in Figs. 3a and 4a, b. However, with further increasing P_{Ar}, the weakening in the couple of Tb with (FeCo) decreases PMA, which results in the decrease of $\mu_0 H_c$ because the weaker PMA makes it easier to reverse magnetic moments. When $P < 52$ W, a surface adatom energy induced by ion/neutron incident at the film increases with the increase in P, which decreases domain wall pinning controlled by the defect and then decreases coercivity. As sputtering power increases from 52 to 64 W, though a surface adatom energy induced by ion/neutron incident at the film surface increases, the adatom has not a selective character because its energy is in excess of threshold energies inducing strong PMA, which is shown in Fig. 4f–h. The weakening of PMA which may also be related to stress induced during deposition for compressive stress is expected due to the formation of perpendicular domains to minimize magneto-elastic energy [12]. The weaker the PMA, the less compressive stress, the lower the magnetic field required to move magnetic domain wall. Consequently, the reverse of the magnetic moment can be achieved at a low magnetic field, which reduces the coercivity. In addition, Cheng [14] thought that a large $\mu_0 H_c$ can be the result of the columnar microstructure of films. The influence factors of the coercivity are complicated; therefore, a further study is needed.

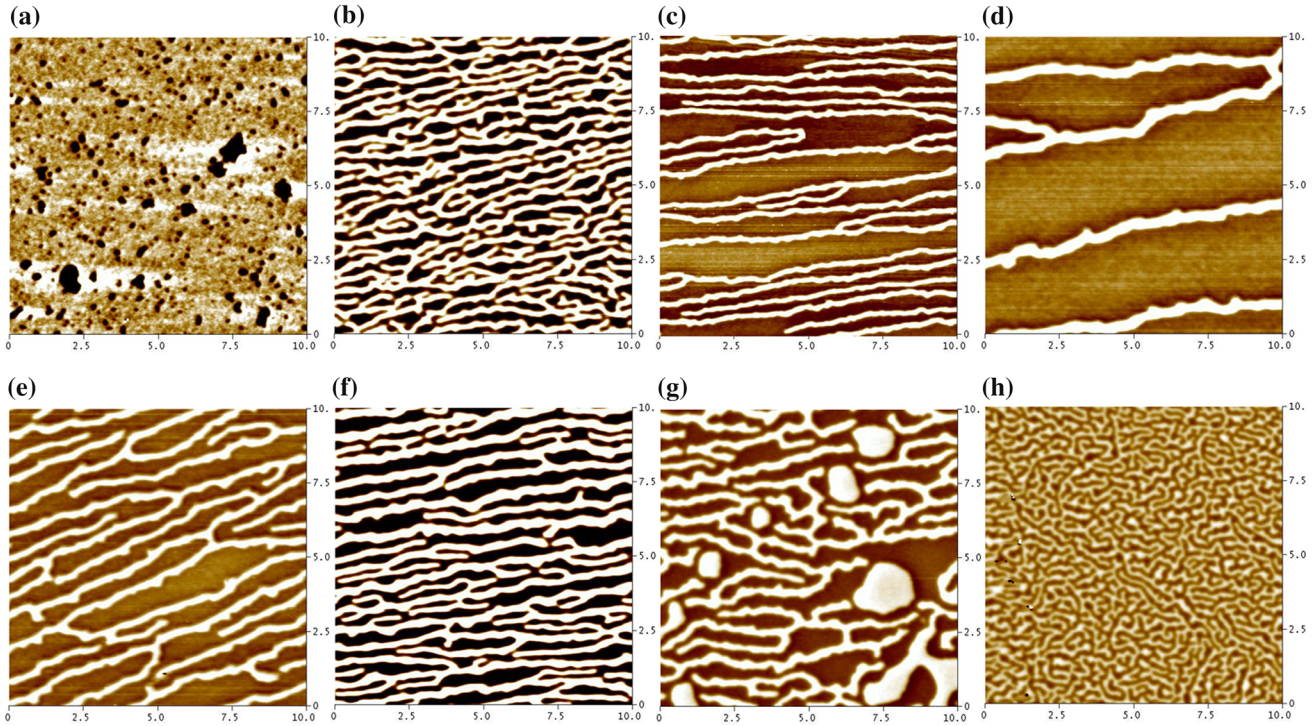

Fig. 4 MFM images of $Tb_{40}(FeCoV)_{60}$ films deposited at P_{Ar}: **a** 0.5 Pa, **b** 0.9 Pa, **c** 1.2 Pa and **d** 1.5 Pa and P: **e** 49 W, **f** 52 W, **g** 58 W and **h** 64 W

Conclusions

The magnetic behaviours of the $Tb_x(Fe_{49}Co_{49}V_2)_{100-x}$ films deposited at different sputtering conditions have been investigated. The composition, magnetic properties and magnetic domain are dominated by adjusting sputtering Ar pressure and power. The magnetic characteristics controlled by process parameters can have a potential application in microactuators and sensors.

Acknowledgements This work is supported in part by the National Natural Science Foundation of China (Project No. 11204147), ZJNSF (Project No. LY13A040002) and NBNSF (Project No. 2013A610130).

References

1. Lee HS, Cho C, Chang SP (2007) Effect of SmFe and TbFe film thickness on magnetostriction for MEMS devices. J Mater Sci 42:384–388. doi:10.1007/s10853-006-1183-4
2. Lee HS, Kim TW (2014) Influence of Ni thin layer on a static and dynamic magnetostrictive behavior in TbFe multi-layered film. Thin Solid Films 562:549–553
3. Feng TF, Chen ZY (2012) Thermal stability of magnetic characteristics in $Tb_{40}(FeCoV)_{60}$ films. Appl Surf Sci 258:5511–5515
4. Mukherjee S, Kreuzpaintner W, Stahn J, Zheng JG, Bauer A, Böni P, Paul A (2015) Exchange-bias-like coupling in a Cu-diluted-Fe/Tb multilayer. Phys Rev B 91:104419
5. Sakurai H, Ota M, Liu X, Morisako A, Sakurai Y, Itou M, Nagao T, Koizumi A (2007) Perpendicular magnetic anisotropy in TbFeCo films studied by magnetic compton scattering. J Appl Phys 102:013902
6. Murakami M, Birukawa M (2008) Sputtering gases and pressure effects on the microstructure, magnetic properties and recording performance of TbFeCo films. J Magn Magn Mater 320:608–611
7. Fellman F, Messer M, Abarra EN (1999) Coercivity in amorphous Tb–Fe alloys. J Appl Phys 86:1047–1052
8. Hellman F (1991) Measurement of magnetic anisotropy of ferrimagnets near compensation. Appl Phys Lett 59:2757–2759
9. Choi YS, Lee SR, Han SH, Kim HJ, Lim SH (1997) The magnetic properties of Tb-Fe-(B) thin films fabricated by rf magnetron sputtering. J Alloys Compd 258:155–162
10. Harris VG, Pokhil T (2001) Selective-resputtering-induced perpendicular magnetic anisotropy in amorphous TbFe films. Phys Rev Lett 87:067207
11. Shih JC, Chin TS, Sun ZG, Zhang HW, Shen BG (2001) Domain structure of TbFe magnetostrictive films by MFM. IEEE Trans Magn 37:2681–2683
12. Jiang HC, Zhang WL, Zhang WX, Peng B (2010) Effects of argon pressure on magnetic properties and low-field magnetostriction of amorphous TbFe films. Phys B 405:834–838
13. Schmidt J, Skidmore G, Foss S, Dahlberg ED, Merton C (2008) Magnetization reversal processes in perpendicular anisotropy thin film observed with magnetic force microscopy. J Magn Magn Mater 190:81–88
14. Cheng SN, Kryder MH (1991) Separation of perpendicular anisotropy components in dc-magnetron sputtered TbFe amorphous films. J Appl Phys 69:7202–7206